Food and Chemical Toxicology 131 (2019) 110529

Contents lists available at ScienceDirect

Food and Chemical Toxicology

journal homepage: www.elsevier.com/locate/foodchemtox

Computational de-orphanization of the olive oil biophenol oleacein: Discovery of new metabolic and epigenetic targets

Elisabet Cuyàs[a,b], David Castillo[c], Laura Llorach-Parés[d], Jesús Lozano-Sánchez[e,f], Sara Verdura[a,b], Alfons Nonell-Canals[d], Joan Brunet[g,h,i,j], Joaquim Bosch-Barrera[b,g,h], Jorge Joven[k], Rafael Valdés[c], Melchor Sanchez-Martinez[d], Antonio Segura-Carretero[e,f], Javier A. Menendez[a,b,*]

[a] ProCURE (Program Against Cancer Therapeutic Resistance), Metabolism & Cancer Group, Catalan Institute of Oncology, Girona, Spain
[b] Girona Biomedical Research Institute (IDIBGI), Girona, Spain
[c] Dreamgenics, Oviedo, Spain
[d] Mind the Byte, Barcelona, Spain
[e] Department of Analytical Chemistry, Faculty of Sciences, University of Granada, Granada, Spain
[f] Research and Development Functional Food Centre (CIDAF), PTS Granada, Granada, Spain
[g] Medical Oncology, Catalan Institute of Oncology (ICO), Dr. Josep Trueta University Hospital, Girona, Spain
[h] Department of Medical Sciences, Medical School University of Girona, Girona, Spain
[i] Hereditary Cancer Programme, Catalan Institute of Oncology (ICO), Bellvitge Institute for Biomedical Research (IDIBELL), L'Hospitalet del Llobregat, Barcelona, Spain
[j] Hereditary Cancer Programme, Catalan Institute of Oncology (ICO) Girona Biomedical Research Institute (IDIBGI), Girona, Spain
[k] Campus of International Excellence Southern Catalonia, Unitat de Recerca Biomèdica, Hospital Universitari de Sant Joan, Institut d'Investigació Sanitària, Pere Virgili, Universitat Rovira i Virgili, Reus, Spain

ARTICLE INFO

Keywords:
Olive oil
Oleacein
Chemoinformatics
Metabolism
Epigenetics

ABSTRACT

The health promoting effects of extra virgin olive oil (EVOO) relate to its unique repertoire of phenolic compounds. Here, we used a chemoinformatics approach to computationally identify endogenous ligands and assign putative biomolecular targets to oleacein, one of the most abundant secoiridoids in EVOO. Using a structure-based virtual profiling software tool and reference databases containing more than 9000 binding sites protein cavities, we identified 996 putative oleacein targets involving more than 700 proteins. We subsequently identified the high-level functions of oleacein in terms of biomolecular interactions, signaling pathways, and protein-protein interaction (PPI) networks. Delineation of the oleacein target landscape revealed that the most significant modules affected by oleacein were associated with metabolic processes (e.g., glucose and lipid metabolism) and chromatin-modifying enzymatic activities (i.e., histone post-translational modifications). We experimentally confirmed that, in a low-micromolar physiological range (< 20 μmol/l), oleacein was capable of inhibiting the catalytic activities of predicted metabolic and epigenetic targets including nicotinamide N-methyltransferase, ATP-citrate lyase, lysine-specific demethylase 6A, and N-methyltransferase 4. Our computational de-orphanization of oleacein provides new mechanisms through which EVOO biophenols might operate as chemical prototypes capable of modulating the biologic machinery of healthy aging.

1. Introduction

The ability of the "Mediterranean diet", which reflects the dietary patterns found in olive-growing areas of the Mediterranean basin, to significantly reduce aging-related morbidity and promote increased life expectancy can be largely attributed to the unique nutraceutical properties of extra virgin olive oil (EVOO) (Colomer and Menendez, 2006; Menendez and Lupu, 2006; Escrich et al., 2007; López-Miranda et al., 2010; Fernández del Río et al., 2016; Piroddi et al., 2017). The positive influence of EVOO on human health has been historically ascribed to its high content of monounsaturated fatty acids (e.g., oleic acid; 18:1n-9). However, it has been shown that other oleic acid-rich oils but lacking the characteristic functional components of EVOO (e.g., biophenols) such as high-oleic canola or high-oleic sunflower oils do not share the same ability to improve, for example, cardiovascular prognosis, and to concurrently lowering the incidence of cancer and neurodegeneration

* Corresponding author. Catalan Institute of Oncology (ICO), Girona Biomedical Research Institute (IDIBGI), Edifici M2, Parc Hospitalari Martí i Julià, E-17190, Salt, Girona, Spain.
E-mail addresses: jmenendez@iconcologia.net, jmenendez@idibgi.org (J.A. Menendez).

https://doi.org/10.1016/j.fct.2019.05.037
Received 14 March 2019; Received in revised form 23 May 2019; Accepted 24 May 2019
Available online 29 May 2019
0278-6915/ © 2019 Elsevier Ltd. All rights reserved.

(Pérez-Jiménez et al., 2007; Visioli and Bernardini, 2011; Menendez et al., 2013; Reboredo-Rodríguez et al., 2018). Accordingly, the pharma-nutritional properties of EVOO are now largely attributed to its unique repertoire of EVOO biophenolic compounds including simple phenols (e.g., tyrosol and hydroxytyrosol) and secoiridoids (e.g., oleuropein aglycone, ligstroside aglycone, oleocanthal, and oleacein).

Although significant efforts have been made to determine the physiological mechanisms regulated by EVOO phenolics, their actual molecular interactors remain largely unknown. Indeed, only a few studies have explored in depth the molecular mechanisms through which EVOO-specific phenolics may provide health benefits (Beauchamp et al., 2005; Vazquez-Martin et al., 2012; Menendez et al., 2013; Corominas-Faja et al., 2018; Pang and Chin, 2018; Verdura et al., 2019). In this regard, we recently envisioned that *in silico*, computational approaches might be particularly useful to elucidate hypothesis-generating pharmacological effects, mechanisms of action, and targets underlying the health-promoting activities of EVOO-related biophenols. Taking advantage of the so-called biological activity spectra (BAS), an intrinsic property of a compound that is largely dependent on its structure and reflects pharmacological effects, physiological, and biochemical mechanisms of action, and specific toxicities, we recently employed PASS (Prediction of Activity Spectra for Substances) software (Lagunin et al., 2000, 2010; Stepanchikova et al., 2003) to analyze the BAS of the complex EVOO secoiridoids oleuropein aglycone and decarboxymethyl oleuropein aglycone (oleacein) (Corominas-Faja et al., 2014). This approach highlighted a number of putative pharmacological effects (e.g., anti-oxidant, anti-inflammatory, anti-neoplastic, and chemopreventive) that might underlie the health-promoting effects of some EVOO biophenols, but the overall picture remained incomplete with regards to their mechanism of action at the molecular level.

We here hypothesized that a reverse pharmacology computational approach might be helpful to "de-orphanize" endogenous ligands and assign molecular functions to EVOO biophenols. Because the oleuropein degradation product oleacein (dialdehydic form of decarboxymethyl elenolic acid linked to hydroxytyrosol; 3,4-DHPEA-EDA) is one of the most abundant EVOO secoiridoids and has been proposed as the key effector of the nutritional and beneficial effects of EVOO given its capacity to survive to the acidic conditions of stomach and be available for absorption into the systemic circulation (Nardi et al., 2014; Costanzo et al., 2018; Corominas-Faja et al., 2018; Lombardo et al., 2018; Celano et al., 2019), we decided to use a systematic chemoinformatics approach coupled to laboratory-based confirmatory testing to discover new biomolecular targets through which oleacein might operate as a poly-therapeutic tool capable of modulating the biologic machinery of healthy aging.

2. Results

We used a virtual profiling approach employing the structure-based software *Ixchel* (Cuyàs et al., 2018a,b), which can perform docking calculations of a given molecule against a database of ~9000 binding sites protein cavities (curated from RSCB PDB according to the UniProtKB human entries) and returns the binding energy of every possible interaction. Through this approach we identified 1251 putative targets. Using a binding energy "significance" threshold of −6.0 kcal/mol to filter the docking-based inverse virtual screening, which was chosen considering the size of the molecule and to ensuring 50% inhibitory concentrations (IC_{50}) values within the physiological micromolar range of oleacein (Xu et al., 2018; Gimeno et al., 2019), we finally selected 996 putative oleacein targets involving > 700 different proteins (Supplementary Table S1).

2.1. Gene enrichment analyses and construction of the oleacein target landscape

To quantitatively assess whether the selected group of targets was more enriched with genes belonging to a specific Gene Ontology (GO) term, or with genes involved in a particular pathway more than would be expected by chance, we utilized Cytoscape, a network visualization and analysis tool, for GO enrichment analyses (Shannon et al., 2003). This included also enrichment analyses of biological pathways and reactions supplied by KEGG, Reactome, and Wikipathways (Supplementary Tables S2 and S3). To validate the Cytoscape-generated annotation of GO terms and KEGG pathways, we used an analogous approach using the Search Tool for the Retrieval of Interacting Genes (STRING), enabling us to evaluate the occurrence of functional domains or conserved sites within the over-represented groups of proteins by including protein signature databases such as INTERPRO and PFAM (Supplementary Tables S2 and S3).

Because the aforementioned approach generated a large number of enriched GO terms, we then used ClueGO, a Cytoscape plug-in that strongly improves biological interpretation of large lists of genes (Bindea et al., 2009) and integrates GO terms as well as KEGG pathways to create functionally organized GO/pathway term networks maintaining the most significant term as the group representative (Supplementary Tables S4, S5, S6, S7).

A visualization of the GO enrichment analysis for putative oleacein targets regarding biological process (BP), cellular compartment (CC), and molecular function (MF) is shown in Fig. 1. Among these terms, peptidyl-amino acid modification, membrane raft, and protein kinase activity were the most significant in the BP, MF, and CC groups, respectively. Also, candidate proteins were enriched in terms of histone phosphorylation (BP), caveola (CC), and histone kinase activity (MF). We then performed pathway enrichment analysis to assess the gene-associated pathways potentially targeted by oleacein (Fig. 2). Overall, the greatest number of proteins were involved in central carbon metabolism in cancer (Fig. 2; supplementary File S8) (Luo and Brouwer, 2013). A circus plot summarizing the relationships between effectors within KEGG pathways and the functions triggered by them is shown in Fig. 3.

Fig. 4 illustrates the GO maps for BP, CC, and MF terms, with each node representing a specific GO term and links between nodes illustrating the interaction between GO terms. The GO map for BP included numerous metabolic processes, whereas caveolae/raft membrane microdomains and cytoplasmic vesicle dominated the CC and MF GO maps, respectively. Fig. 5 shows a visualization of the oleacein target landscape using a circle-packing graph of core proteins grouped into higher order functions, in which the circles are sized by relative abundances of proteins contributing to each function. This analysis supports the notion that oleacein preferentially targets metabolic-related processes and histone-related functions.

2.2. Experimental validation of oleacein-targeted metabolic and epigenetic targets

We finally selected four different metabolic and epigenetic enzymes, namely nicotinamide N-methyltransferase (NNMT), which catalyzes the N-methylation of nicotinamide, pyridines, and other analogs using S-adenosyl-l-methionine (SAM) as donor (Hoshino et al., 1982), ATP-citrate lyase (ACLY), a cytoplasmic enzyme that catalyzes the production of acetyl-CoA from citrate, CoA, and ATP (SRERE, 1959), lysine-specific demethylase 6A/UTX (KDM6A) (Agger et al., 2007), which acts as a component of the COMPASS complex to control gene activation by catalyzing demethylation of H3K27me2/3 in the chromatin of genes and enhancers, and DOT1L (also called lysine N-methyltransferase 4), a SAM-dependent methyltransferase that can add up to three methyl groups to histone H3 lysine 79 (H3K79) (Feng et al., 2002), to computationally rationalize the binding mode of oleacein and experimentally verify *in vitro* its inhibitory activity towards them.

Fig. 6 summarizes the overall structure and detailed views of the pharmacophoric interactions between oleacein and NNMT (Fig. 6A), ACLY (Fig. 6B), KDM6A/UTX (Fig. 6C), and DOT1L (Fig. 6D). Table 1

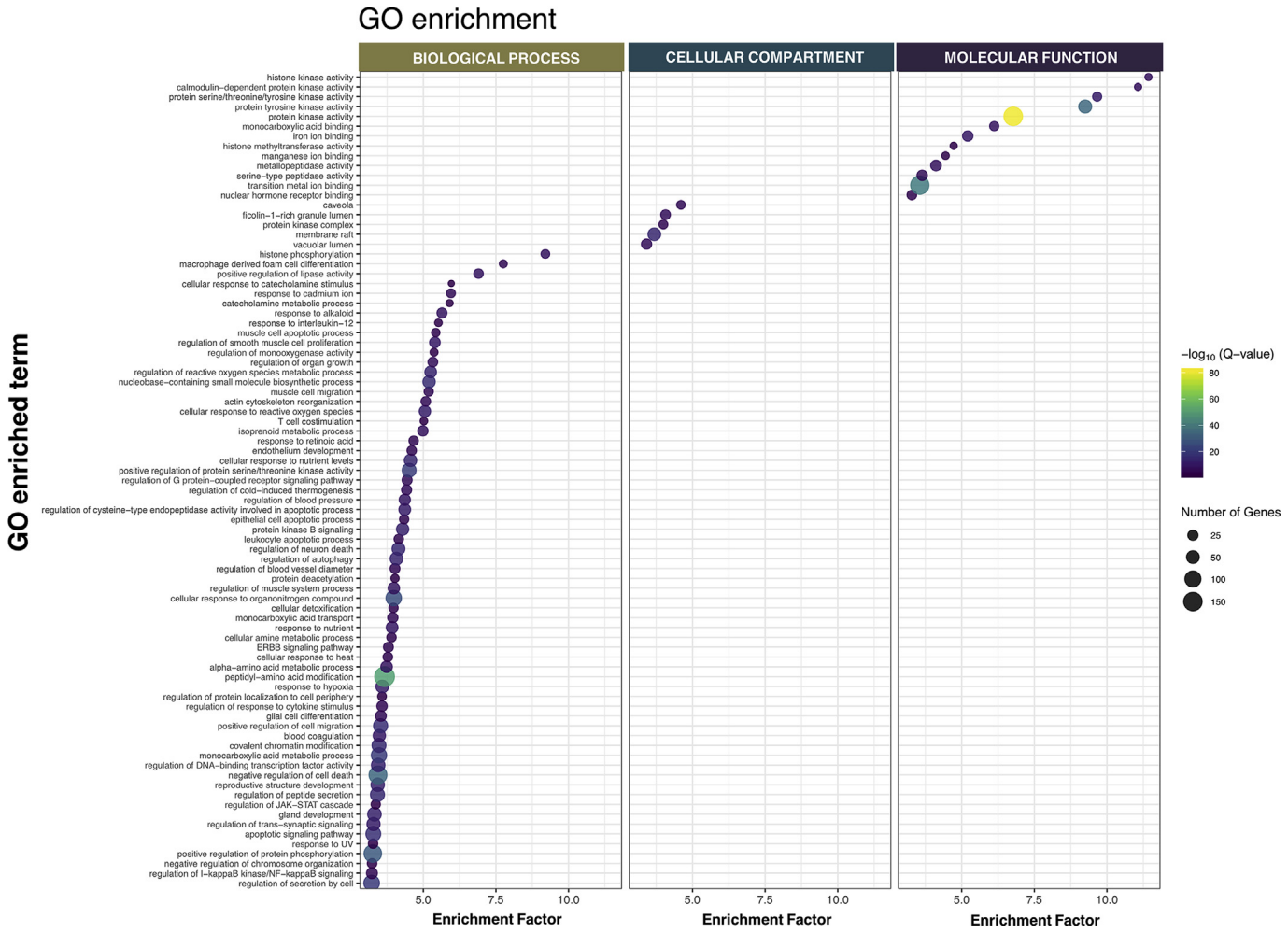

Fig. 1. GO enrichment analysis of VP-based oleacein targets. Bubble plot visual representation of the GO Biological Process (BP), Cellular Component (CC), and Molecular Function (MF) enrichment analyses. In total, 590 genes were identified to have functional annotations based on GO Biological Process EBI-UniProt dataset (version 01.02.2019). Upon applying q-value significance selection criteria, 377 BP, 13 CC, and 28 MF terms were found to be enriched, which distributed into 65 BP, 5 CC, and 13 MF groups according to their gene and kappa coefficient agreement. The y-axis shows the enriched group representatives, the x-axis corresponds to the enrichment factor, the color of the bubbles represents the -$\log_{10}$(q-value) and their size corresponds to the number of genes in the analysis associated with the term. (For interpretation of the references to color in this figure legend, the reader is referred to the Web version of this article.)

summarizes the predicted interacting residues involved in the binding mode of oleacein to NNMT, ACLY, KDM6A/UTX, and DOT1L as well as the docking binding energies (in kcal/mol) and Molecular Mechanics (MM)/General Born Surface Area (GBSA)-based energy rescoring calculations over molecular dynamics (MD) simulations, which takes into consideration the dynamic nature of predicted targets and it is therefore more reliable to provide a realistic view of oleacein binding affinity than the rigid docking calculations. The MM/GBSA approximation highlighted a high affinity of oleacein towards NNMT, ACLY, KDM6A/UTX, and DOT1L, which reached energy bindings > 30 kcal/mol in all cases. Table 2 summarizes the mean IC_{50} values of oleacein obtained from the different *in vitro* studies carried out with purified enzymes. Low-micromolar concentrations of oleacein (< 15 μM) were found to efficiently inhibit the *in vitro* activities of NNMT, ATPCL, KDMA6A/UTX, and DOT1L enzymes (Fig. 7, Table 2).

3. Discussion

EVOO biophenols constitute biologically pre-validated chemical prototypes capable of interacting with health-promoting molecular targets. However, although it is widely accepted that the chemical architectures of natural products might offer unique opportunities for drug discovery, the bulk of the chemical environment specifically present in the phenolic fraction of EVOO is essentially uncharted. We here provide biocomputational evidence to suggest that the capacity of the EVOO secoiridoid oleacein to provide health benefits likely involves a significant number of metabolic and epigenetic targets.

Proteomics is the technology most commonly employed for identifying molecular binding counterparts for naturally occurring chemotypes. However, target prediction software tools are becoming increasingly useful to assign putative biomolecular targets to natural products. In this line, the virtual profiling structure-based software tool *Ixchel* allowed us to predict that the oleacein scaffold displays potential for engaging almost 1000 putative targets involving more than 700 proteins. Our integrative analysis initially aimed to provide evidence-based statements associating the predicted oleacein targets with specific ontology terms, and to interpret their high-level functions in terms of signaling pathways. Regarding GO annotation, the most significantly enriched terms were associated with cellular protein modification processes. It is noteworthy that protein post-translational modifications (PPMs), either spontaneous or physiological/pathological, are epigenetic mechanisms emerging as critical contributors to aging and aging-related diseases (Santos and Lindner, 2017; Vanhooren et al., 2015). Furthermore, the finding of lipid raft microdomains (caveolae) as the preferential cellular compartment of oleacein, adds a spatial dimension to the PPM nature of oleacein because the key function of caveolae is to

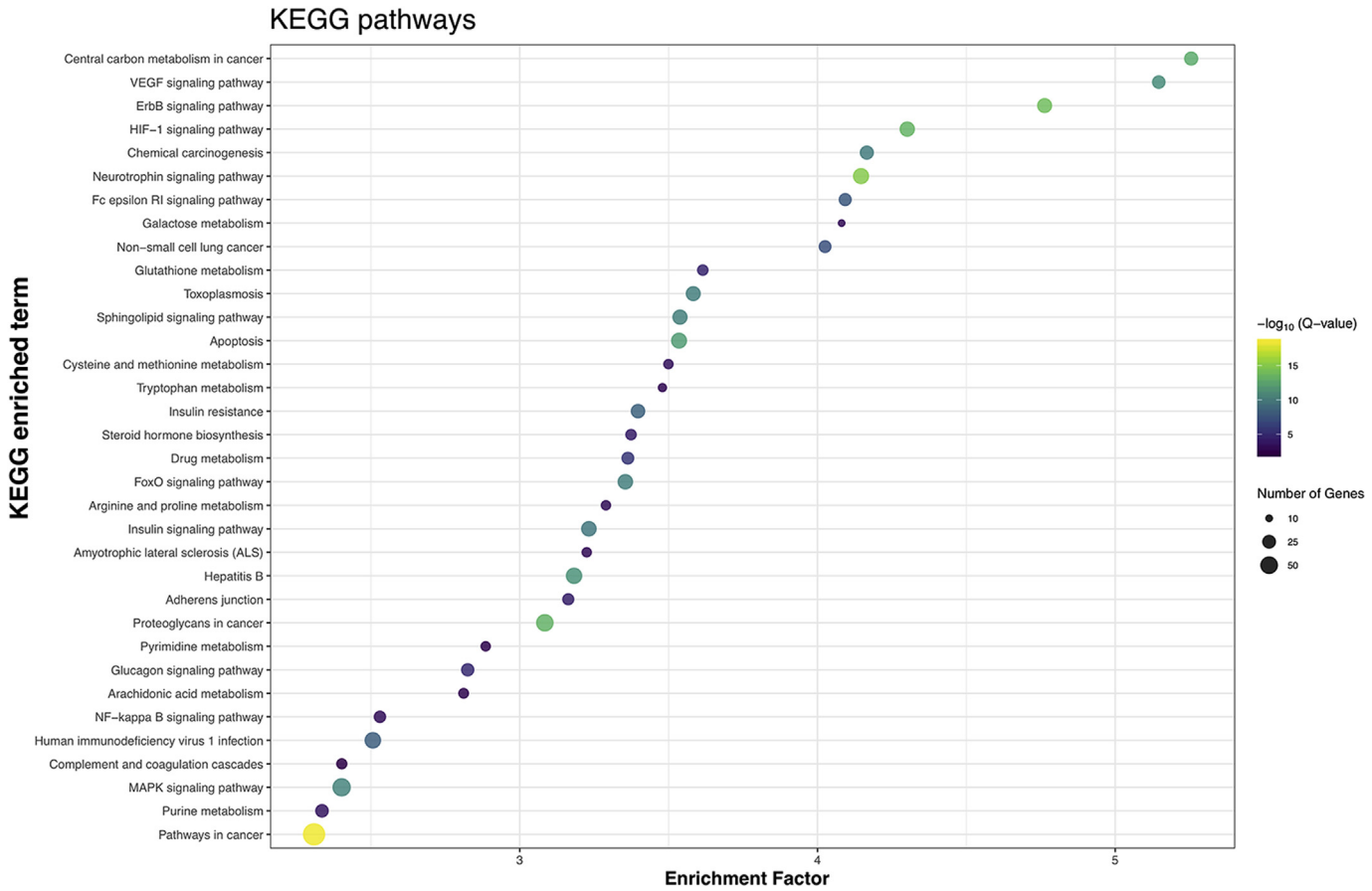

Fig. 2. KEGG pathway analysis of VP-based oleacein targets. Bubble plot visual representation of the KEGG enrichment analysis. In total, 495 genes were identified to have functional annotations based on KEGG dataset (version 01.02.2109). Upon applying q-value significance selection criteria, 119 pathways were found to be enriched, which distributed into 35 groups according to their gene and kappa coefficient agreement. The y-axis shows the enriched group representatives, the x-axis corresponds to the enrichment factor, the color of the bubbles represents the -$\log_{10}$(q-value) and their size corresponds to the number of genes in the analysis associated to the KEGG pathway. (For interpretation of the references to color in this figure legend, the reader is referred to the Web version of this article.)

concentrate signaling molecules, allowing their rapid activation upon demand by PPMs (Ortegren et al., 2007; Layne et al., 2011). These findings support the notion that plant-derived phenolics can target and change the activation status of caveolae-associated signaling proteins, and agree with earlier studies from our group suggesting that EVOO phenolics such as oleacein could accumulate in lipid raft microdomains and subsequently interfere with the dimerization and activation (e.g., auto-phosphorylation) of cancer-related protein tyrosine kinases such as HER2 (Menendez et al., 2008, 2009). Regarding pathway enrichment, the majority of significantly enriched terms were associated with pathways in cancer, whereas the majority of predicted targets were involved in central carbon metabolism in cancer, which is known to involve those proteins providing specific adaptations of cellular metabolism to support growth and survival in cancer cells.

We constructed functional protein association networks with the aim of interpreting the impact of oleacein on complex biological processes. A bird's-eye view of the oleacein target landscape revealed that the most significant modules were associated with metabolic processes (e.g., glucose and lipid metabolism) and chromatin-modifying enzymatic activities (i.e., histone post-translational modifications). These findings agree with and further expand on a previously described cell-based phenotypic drug discovery strategy coupled to mechanism-of-action profiling and target deconvolution demonstrating the ability of oleacein to target cancer stem cells *via* metabolo-epigenetic mechanisms (Corominas-Faja et al., 2018). Nonetheless, because experimental confirmation is required for these predictions, we selected two metabolic (i.e., NNMT and ACLY) and two epigenetic (KDM6A/UTX and DOT1L) processes to directly evaluate the regulatory effects of oleacein. The acetyl-CoA-synthesizing enzyme ACLY, a strategic enzyme linking glycolytic and lipidic metabolism, is known to be aberrantly expressed in many types of tumors, and also to couple changes of intermediate metabolism to the chromatin-mediated regulation of transcription during aging (Wellen et al., 2009; Zaidi et al., 2012; Peleg et al., 2016; Zhao et al., 2016; Granchi, 2018). NNMT impairs the methylation potential of cells and brings about an altered epigenetic state by consuming methyl units from SAM to create the stable metabolic product 1-methylnicotinamide (MNA), which is associated with obesity, type-2 diabetes, cancer, and aging (Ulanovskaya et al., 2013; Kraus et al., 2014; Hong et al., 2015, 2018). The H3K27me3 histone demethylase KDM6A/UTX is a key aging/senescence-related chromatin regulator not only in somatic cells during the normal aging process but also in prematurely aging cells in Hutchinson-Gilford progeria and Werner syndromes (Jin et al., 2011; Maures et al., 2011; Shah et al., 2013; Cuyàs et al., 2018a,b). Finally, DOT1L-mediated H3K79 methylation is a critical epigenetic modification that regulates cell cycle progression, somatic reprogramming, and DNA damage repair and, accordingly, DOT1L inhibitors have the potential to be employed in several forms of cancers and potentially for delaying cancer (Kim et al., 2012, 2014; Nguyen and Zhang, 2011; Anglin and Song, 2013). In this regard it should be noted that oleacein can be absorbed into the systemic circulation where it might reach concentrations up to 20 μM (Lombardo et al., 2018), a plausible exposure concentration capable of physiological inhibiting the experimentally validated metabolo-epigenetic effectors of the health-promoting effects of EVOO.

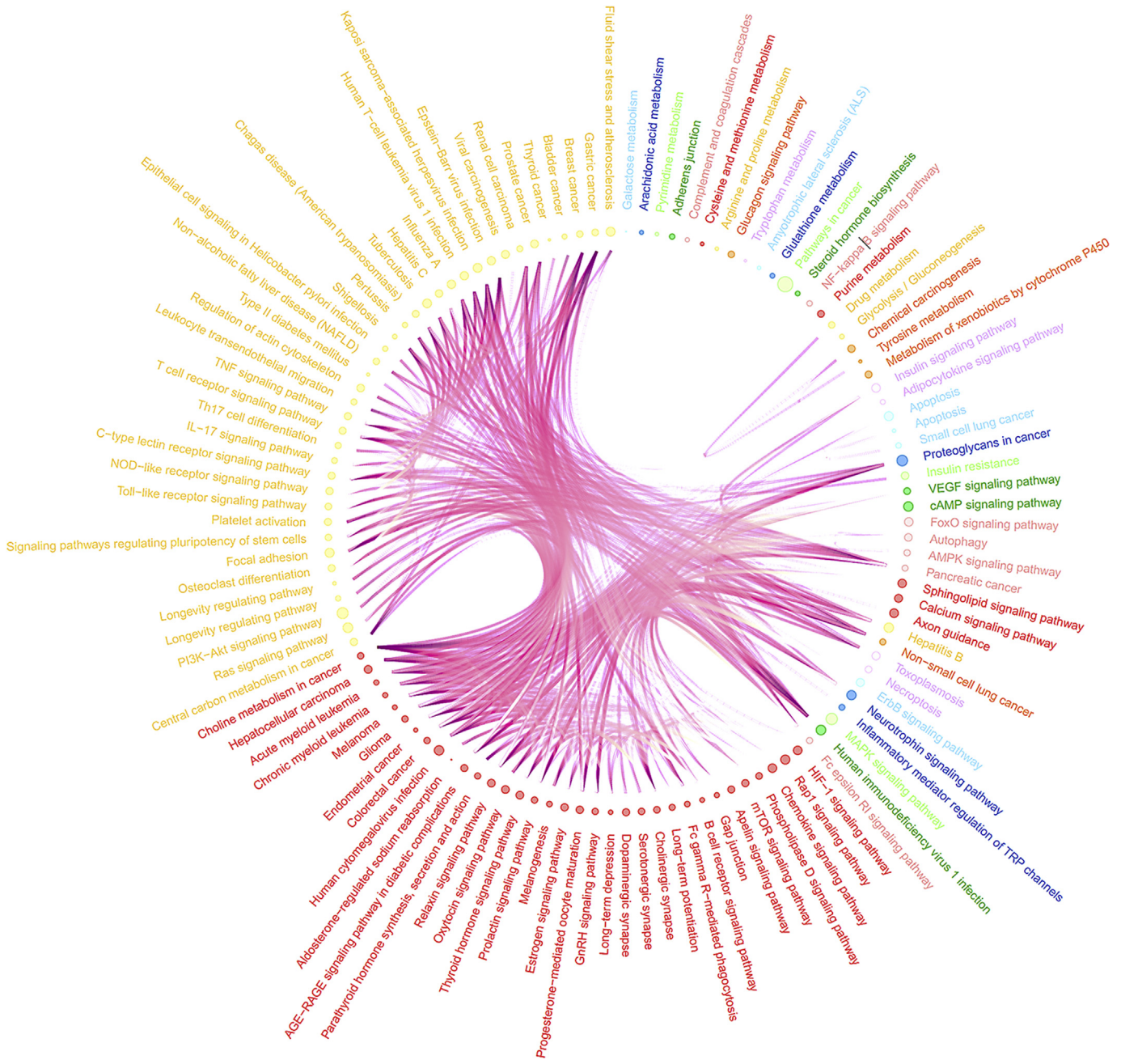

Fig. 3. Hierarchical edge bundling of VP-based oleacein targets. Network representatioon of the KEGG enrichment analysis. Pathways are displayed in a circular layout; relationships between entities and resulting groups are based on their gene and kappa coefficient agreement. Consequently, nodes from the same group are organized adjacent to each other and share the same color. Node size represents the number of genes in the analysis associated with the pathway. (For interpretation of the references to color in this figure legend, the reader is referred to the Web version of this article.)

4. Conclusions

In summary, although significant efforts have been made to clarify the physiological mechanisms regulated by EVOO phenolics, their actual molecular interactors remain largely unknown. Here, we have outlined a first-in-class systematic chemoinformatics approach to computationally predict biomolecular targets of the EVOO secoiridoid oleacein. We provide computational evidence coupled to experimental validation to suggest that one of the most representative EVOO biophenols can operate as a poly-therapeutic tool *via* targeting of metabolic and epigenetic mechanisms. From a pharmacophore perspective, our target de-orphanization of oleacein might illuminate innovative scaffolds that could be employed in rational chemical biology and drug discovery approaches aimed to design new EVOO phenolics-inspired chemical entities.

5. Materials and methods

5.1. Virtual profiling

Virtual profiling was performed with the structure-based software tool Ixchel (http://www.mindthebyte.com), using the chemical structure of oleacein as a seed. Ixchel is a structure-based VP tool that performs docking calculations of a molecule (SDF or SMILE file) against an in-house developed database of almost 9000 binding sites protein cavities curated from RSCB PDB according to UniProtKB human entries.

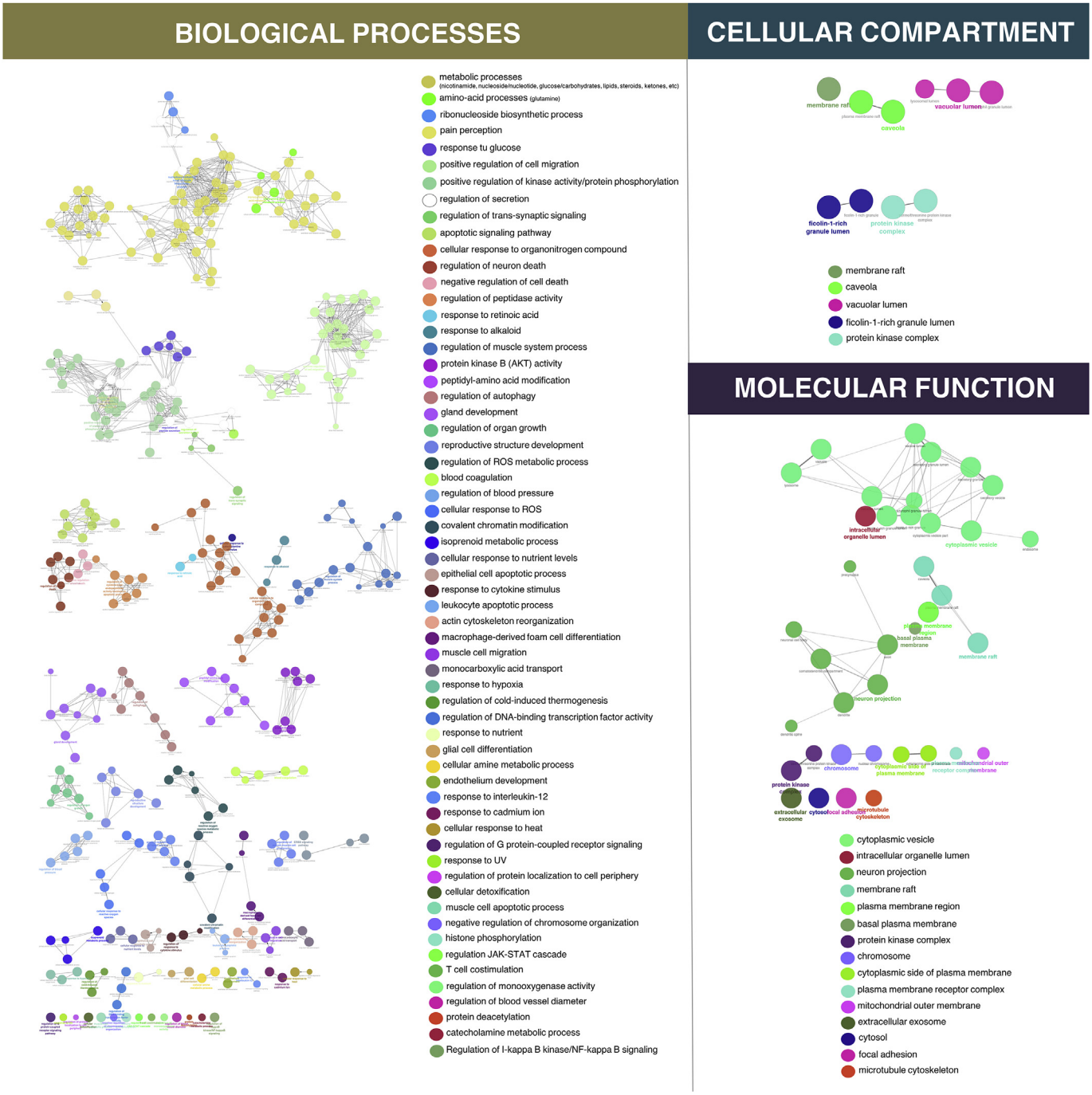

Fig. 4. Protein-protein interaction network analysis of VP-based oleacein targets. ClueGO network representation of the GO BP, CC, and MF enrichment analyses. Terms in the network are shown as nodes while their color and edges are based on their gene and kappa coefficient agreement. The label of the representative group, having the lowest q-value per group, is also shown. Node size represents the term enrichment significance. (For interpretation of the references to color in this figure legend, the reader is referred to the Web version of this article.)

Ixchel returns the binding energy of every possible interaction, which allows the classification and prediction of the targets. Docking calculations, molecular dynamics simulations, binding free energy analysis, and interaction analysis were performed as described elsewhere (Cuyàs et al., 2018a,b; Verdura et al., 2018).

5.2. Gene enrichment analysis

Gene enrichment analysis was performed using ClueGO, a Cytoscape plug-in, interrogating GO terms (Biological Process, Cellular Component and Molecular Function; www.geneontology.org) and KEGG pathways (www.genome.jp/kegg). The selection criteria comprised a two-sided hypergeometric test (enrichment/depletion) followed by a *p*-value correction Bonferroni test, filtering for *q*-values < 0.05. A final step involved grouping terms with more than 25% of common genes with a level of agreement greater than 0.40 based on the Cohen's kappa coefficient. The term with the lowest q-value was designated as group representative.

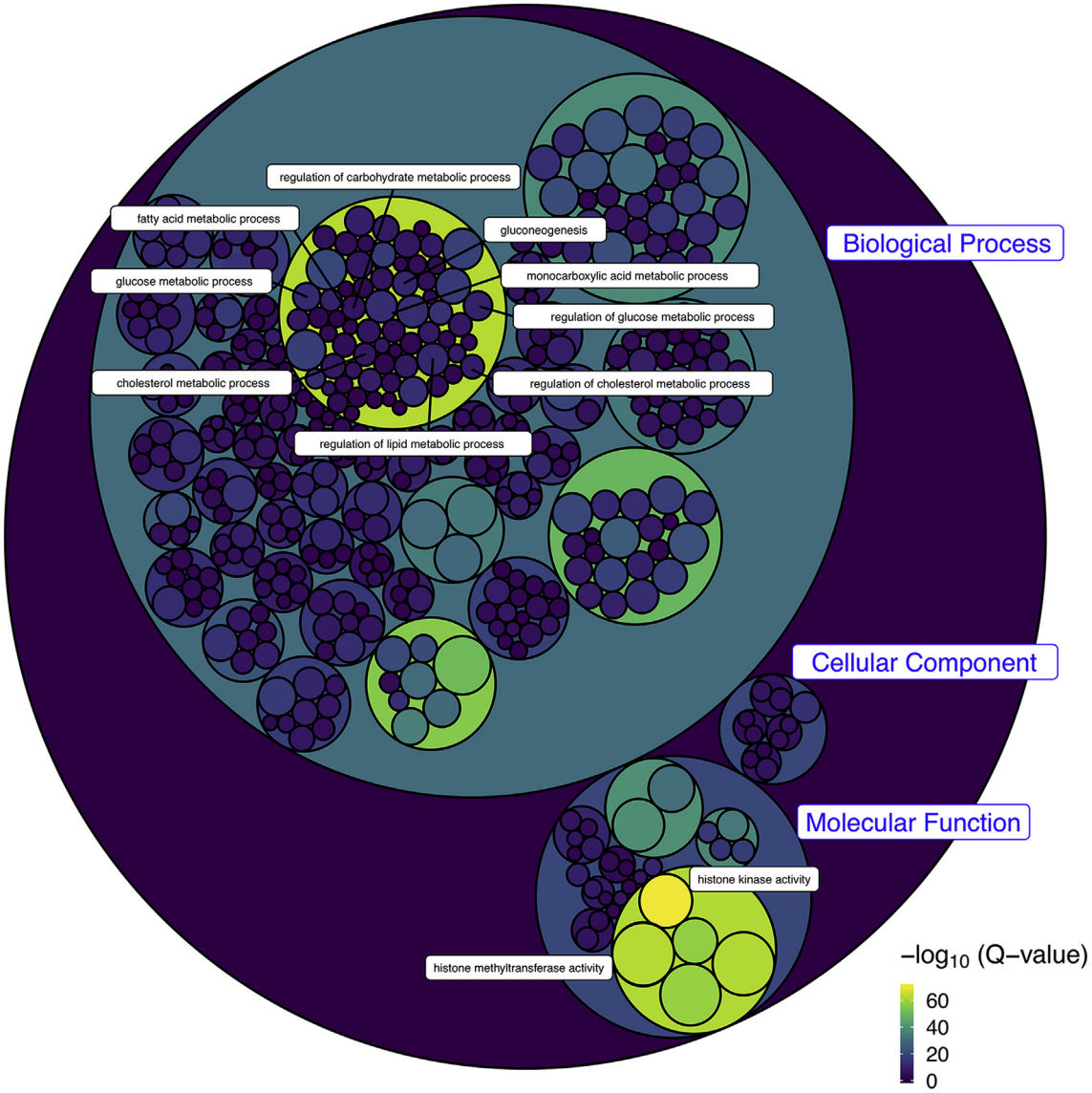

Fig. 5. Visualization of oleacein target ontology. Circle packing, landscape visualization of VP-based oleacein targets including a three-level hierarchical representation of the GO enrichment analyses. The first level corresponds to the GO category (BP, CC, and MF), the second level symbolizes the cluster of terms grouped by gene and kappa coefficient agreement, and the final level represents the individual enriched terms. The color of the bubbles represents the -$\log_{10}$(q-value) and the size of each individual term is proportional to the number of genes found in the analysis. Groups with a single enriched term are displayed in a two-level hierarchy display without group encapsulation. (For interpretation of the references to color in this figure legend, the reader is referred to the Web version of this article.)

5.3. Enzymatic assays

5.3.1. NNMT

NNMT activity was measured using the N′-Nicotinamide Methyltransferase (NNMT) Inhibitor Screening Assay Kit (BioVision, ref. K822) as per the manufacturer's instructions. The IC_{50} value was calculated by interpolation of dose-response curves using GraphPad Prism software (GraphPad Software Inc.).

5.3.2. ACLY

The assay was performed by quantifying the enzymatic activity of recombinant human ACLY (BPS#50255, lot#161226-G) using ADP-Glo luminescence assay reagents. The luminescent signal from the assay correlates with the amount of ADP consumed and proportionally correlates with the amount of ACLY activity.

Oleacein was diluted in 10% DMSO and 2.5 μL of the dilution was added to 22.5 μL of reaction mix such that the final DMSO concentration was 1% in all of the reactions. All of the enzymatic reactions were conducted at 30 °C for 60 min. The 25 μL reaction mixture contained 40 mM Tris, pH 8.0, 10 mM $MgCl_2$, 5 mM DTT, 100 μM ATP, 200 μM CoA, and 200 μM sodium citrate, and 30 ng/reaction of ACLY. Twenty-five microliters of the ADP-Glo reagent was added at the end of each reaction and the plate was incubated for 45 min at room temperature (RT). Fifty microliters of Kinase Detection Reagent was then added and the reaction was incubated for a further 60 min at RT. The luminescence signal was measured using a BioTek Synergy 2 microplate reader.

ACLY activity assays were performed in duplicate at each concentration. The luminescence data were analyzed using Graphpad Prism software (GraphPad Software Inc.). The difference between luminescence intensities in the absence of ACLY (Lu_t) and in the presence of ACLY (Lu_c) was defined as 100% activity (Lu_t - Lu_c). Using the luminescence signal (Lu) in the presence of oleacein, the % activity was calculated as: % activity = $[(Lu_t - Lu)/(Lu_t - Lu_c)] \times 100\%$ (all percent activities below zero where considered zero in the analysis). To calculate the IC_{50} value, the values of % activity versus a series of oleacein concentrations were plotted using non-linear regression analysis of

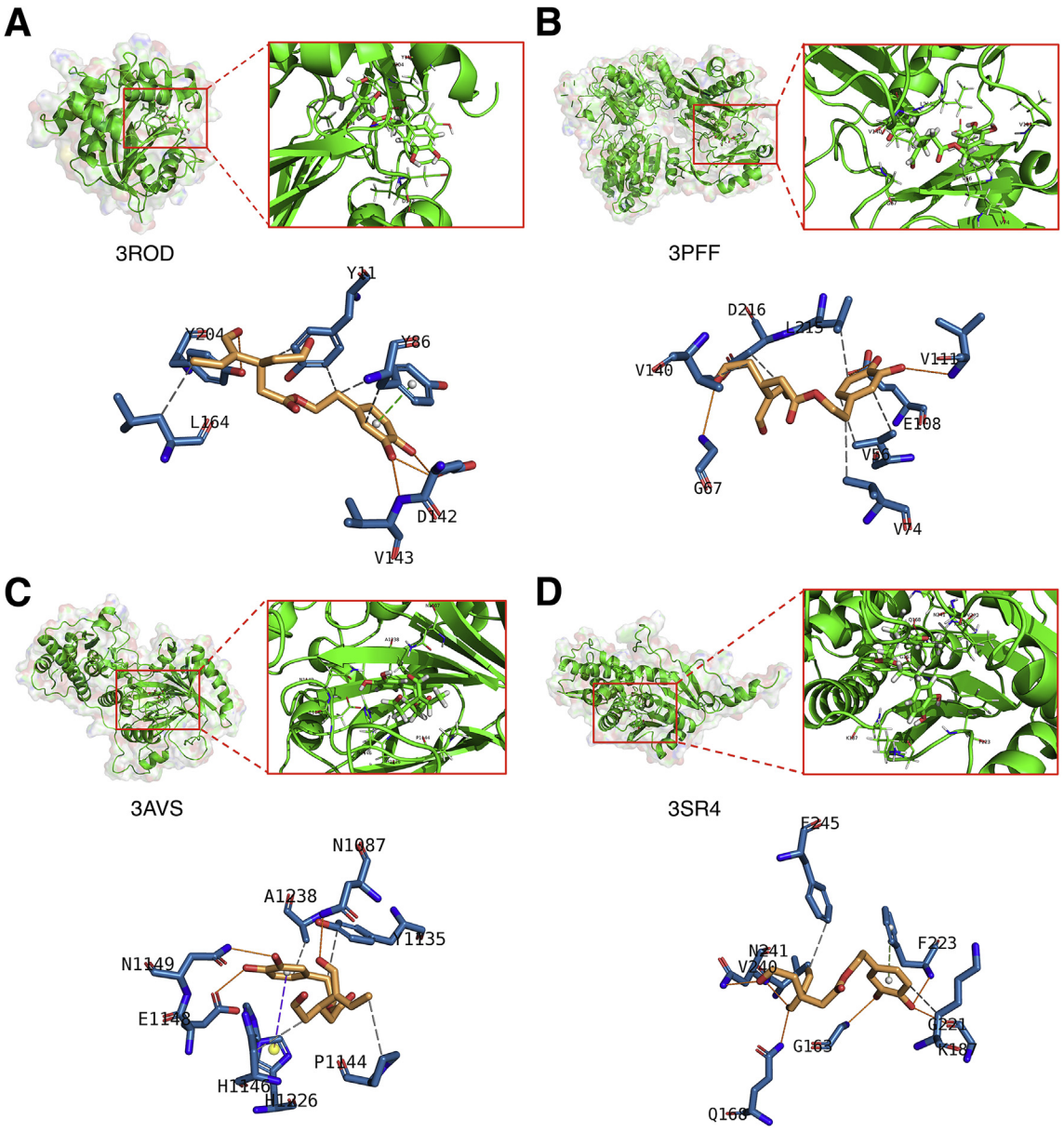

Fig. 6. Binding modes of oleacein to NNMT, ACLY, KDM6A/UTX, and DOT1L. Overall structure and detailed views of the pharmacophoric interactions between oleacein and NNMT, ACLY, KDM6A/UTX, and DOT1L, using PLIP. Orange dashed lines represent hydrogen bond interactions; gray dashed lines represent hydrophobic interactions. The main coordinating residues involved in oleacein interaction with the respective protein backbones are shown in black; the residue numbers correspond to the original PDB file numbering. **A.** Using the PDB crystal structure 3ROD, oleacein was predicted to target the NNMT active site occupied by S-adenosylhomocysteine (SAH), the SAM demethylated product, likely interfering with NNMT catalysis. Interactions with TYR86, ASP142 and VAL143 were revealed by molecular dynamics (MD) simulations as key interacting residues and SAH binders, establishing hydrogen bonds (ASP142 and VAL143), hydrophobic interactions (TYR86) and a π-π stacking interaction at the benzene oleacein ring. Another residue, TYR204, stabilized the molecule on the opposite site, which established hydrogen bonds and hydrophobic interactions with TYR11 and LEU164, respectively. **B.** Using the PDB 3PFF crystal structure with the co-crystal ligand ADP of ACLY, six residues were identified as key binders after docking and MD simulations. Four of them, VAL56, VAL74, VAL111 and LEU215, stabilized the oleacein molecule by establishing both hydrophobic interactions and hydrogen bonds at the benzene ring, whereas VAL140 and ASP216 stabilized the tail region through hydrophobic interactions. Furthermore, VAL111 and ASP216 were key residues for ADP binding. Residues GLY67 and GLU108 were also revealed after MD simulations, both establishing hydrogen bonds with the molecule. **C.** The KDM6A/UTX crystal structure PDB 3AVS revealed the capacity of oleacein to bind to its catalytic cavity. Although oleacein was predicted not to share any interacting residues with 2-oxoglutarate (α-ketoglutaric acid), the crystallographic ligand, docking calculations and MD simulations revealed its interaction with important residues placed nearby, including ASN1087 and ASN1149, which stabilized the molecule by establishing hydrogen bonds interactions, and with HIS1146, establishing hydrophobic interactions. Four other residues were revealed to be involved in oleacein binding: TYR1135, PRO1144 and ALA1238 established hydrophobic interactions and GLU1148 established hydrogen bonding. **D.** Using the PDB crystallographic structure 3SR4 of DOT1L containing the co-crystal ligand TT8, oleacein was predicted to establish hydrogen bond interactions with GLY221, PHE223 and ANS241. Additionally, PHE223, stabilized the benzene ring establishing a π-π stacking interaction. Hydrophobic interactions were established by LYS187 and PHE245. This group of residues was maintained after docking and MD simulations, and also LYS187 and PHE223 were revealed to be key residues as both are involved in TT8 binding. Another group of residues interacting with oleacein after the MD simulations were GLY163, GLN168 and VAL240, and all stabilized the molecule by establishing hydrogen bonds interactions. (For interpretation of the references to color in this figure legend, the reader is referred to the Web version of this article.)

Table 1
Binding mode of oleacein to metabolic and epigenetic targets. Interacting residues that are meant to establish key interactions with oleacein are highlighted. Docking binding energies (in kcal/mol) and Molecular Mechanics (MM)/General Born Surface Area (GBSA)-based energy rescoring calculations over molecular dynamics (MD) simulations of oleacein against DOT1L, ACLY, NNMT, and KDM6A/UTX are shown. The more negative the binding energy, the more plausible the interaction.

3SR4 (DOT1L) Residues		3PFF (ACLY) Residues		3ROD (NNMT) Residues		3AVS (KDM6A) Residues	
Docking	MD	Docking	MD	Docking	MD	Docking	MD
LYS 187	GLY 163	VAL 111	VAL 111	TYR 204	VAL 143	ASN 1087	ASN 1087
PHE 223	ASN 241	LYS 58	GLY 67	THR 144	TYR 204	ASN 1149	ASN 1149
GLY 137	GLN 168	VAL 72	GLU 108	VAL 143	ASP 142	ASN 1148	GLU 1148
GLY 221	PHE 223	LEU 215	VAL 56	ASN 90	TYR 86	1149	PRO 1144
ASP 222	GLY 221	ASP 216	VAL 74	ASP 142	LEU 164	GLY	HIS 1146
PHE 245	LYS 187	VAL 74	LEU 215	TYR 86	TYR 11	1128	TYR 1135
TYR 136	VAL 240	PHE 110	VAL 140	PHE 15		HIS 1146	ALA 1238
ASN 241	PHE 245	VAL 56	ASP 216	LYS 8		ARG	
		VAL 140		ALA 169		1001	

Energy (DOT1L)		Energy (ACLY)		Energy (NNMT)		Energy (KDM6A)	
Docking	MM/GBSA	Docking	MM/GBSA	Docking	MM/GBSA	Docking	MM/GBSA
-7.7/-7.7	-35.5902	-7.1/-7.1	-31.9313	-8.8/-8.8	-41.8110	-7.3/-7.3	-30.4939

Table 2
IC_{50} values (μM) of oleacein for inhibition of VP-predicted metabolic and epigenetic enzymes.

Enzyme	oleacein IC_{50} value (μM)
NNMT	8.9
ACLY	9.1
KDM6A/UTX	7.1
DOT1L	14.1

sigmoidal dose-response curve generated with equation $Y = B + (T-B)/1 + 10^{((LogEC50 - X) \times Hill\ Slope)}$, where Y = percent activity, B = minimum percent activity, T = maximum percent activity, X = logarithm of compound and Hill Slope = slope factor or Hill coefficient. The IC_{50} value was determined as the concentration causing a half-maximal percent activity.

5.3.3. DOT1L

All the enzymatic reactions were conducted in duplicate at RT for 120 min in a 50-μL reaction mixture containing HMT assay buffer (BPS#52180), the SAM cofactor (5 μM; BPS#52120), recombinant human DOT1L (BPS#50105, lot#120110), and oleacein. Reactions were carried out in wells pre-coated with a DOT1L substrate (0.3 μM). The final DMSO concentration was 1%.

After the enzymatic reaction, the reaction mixtures were discarded and each well was washed three times with TBST buffer and slowly

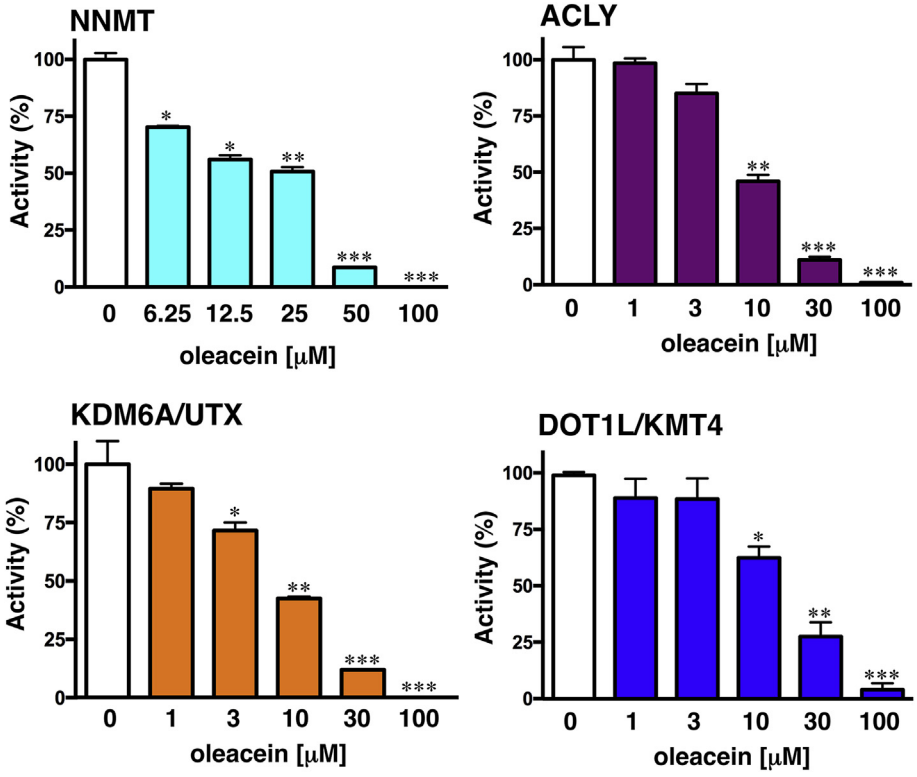

Fig. 7. Oleacein effects on NNMT, ACLY, KDM6A/UTX, and DOT1L enzymatic activities. **A**. NNMT activity was measured by indirectly quantifying the amount of SAH generated during the methylation of nicotinamide by NNMT enzyme in the absence and presence of graded concentrations of oleacein. **B.** ACLY activity was measured by quantifying the amount of ADP produced by the enzymatic reaction in the absence and presence of graded concentrations of oleacein. **C.** KDM6A/UTX demethylase activity on a histone H3 peptide was measured using an AlphaScreen assay in the absence and presence of graded concentrations of oleacein. **D.** SAM-dependent DOT1L/KMT-driven methyltransferase activity was measured by chemiluminiscent assays measuring the methylated K79 residue of H3. Columns and error bars represent mean values and S.D., respectively. Data are representative of at least two independent experiments as the function of oleacein concentrations. (* $P < 0.05$; ** $P < 0.01$; *** $P < 0.001$).

shaken with blocking buffer (BPS#52100) for 10 min. The wells were emptied and 100 μL of diluted primary antibody in blocking buffer (BPS#52140Y) was added, and the plate was slowly shaken for 10 min at RT. After removal of the primary antibody mix, 100 μL of diluted HRP-labeled secondary antibody (BPS#52131H) was added and the plate was slowly shaken for 30 min at RT. As before, the plate was emptied and washed three times with blocking buffer for 10 min at RT. Blocking buffer was finally discarded and 100 μL of freshy prepared HRP chemiluminiscent substrate was added to each well. Luminescence was immediately measured using a BioTek Synergy 2 microplate reader. Luminescence data were converted to DOT1L activity (%) and the IC_{50} value was determined as mentioned above.

5.3.4. KDM6A/UTX

Enzymatic reactions were performed in an AlphaScreen format in duplicate at RT for 60 min in a 10 μL mixture containing assay buffer, histone H3 peptide substrate, KDM6A/UTX (BPS#50116, lot#150805-A) enzyme, and oleacein. The 10-μL reactions were carried out in 384-well Optiplates (PerkinElmer). Serial dilution of the compounds was first performed in 3.3% DMSO/assay buffer. From this step, 3 μL of compound is added to 4 μL of enzyme and is incubated for 30 min at RT. After this incubation, 3 μL of substrate is added to initiate the reaction. The final DMSO concentration is 1%. After enzymatic reactions, 5 μL of anti-mouse acceptor beads (PerkinElmer, diluted 1:500 with 1 × detection buffer) or 5 μL of anti-rabbit acceptor beads (PerkinElmer, diluted 1:500 with 1 × detection buffer) and 5 μL of primary antibody (BPS#52140E,F, diluted 1:200 with 1x detection buffer) were added to the reaction mix. After brief shaking, the plate was incubated for 30 min. Finally, 10 μL of AlphaScreen streptavidin-conjugated donor beads (Perkin, diluted 1:125 with 1 × detection buffer) were added. After 30 min, the samples were measured in the AlphaScreen microplate reader (EnSpire Alpha 2390 Multilabel reader, PerkinElmer).

The AlphaScreen intensity data were analyzed and compared using Graphpad Prism software (GraphPad Software Inc.). In the absence of oleacein, the A-screen or fluorescence intensity (F_t) was defined as 100% activity. In the absence of enzyme, the intensity (F_b) was defined as 0% activity. The percent activity in the presence of oleacein was calculated according to the following equation: %activity = $(F\text{-}F_b)/(F_t\text{-}F_b)$, where F = the A-screen intensity in the presence of oleacein. A-screen data were converted to KDM6A/UTX activity (%) and the IC_{50} value was determined as mentioned above.

5.4. Statistical analysis

All statistical analyses were performed using GraphPad Prism software (GraphPad Software Inc.). Data are presented as mean ± S.D. Comparisons of means of ≥3 groups were performed by ANOVA with the post-hoc Bonferroni correction when appropriate. P values < 0.05 were considered to be statistically significant (denoted as *). All statistical tests were two-sided.

Declaration of interests

The authors declare that they have no known competing financial interests or personal relationships that could have appeared to influence the work reported in this paper.

Acknowledgments

Work in the Menendez laboratory is supported by the Spanish Ministry of Science and Innovation (Grant SAF2016-80639-P, Plan Nacional de I+D+I, founded by the European Regional Development Fund, Spain) and by an unrestricted research grant from the Fundació Oncolliga Girona (Lliga catalana d'ajuda al malalt de càncer, Girona). The authors would like to thank Dr. Kenneth McCreath for editorial support. This work is in loving memory of Àlex Casta, a generous, kind, and cheerful friend and colleague who passed away in December 2018.

Appendix A. Supplementary data

Supplementary data to this article can be found online at https://doi.org/10.1016/j.fct.2019.05.037.

Transparency document

Transparency document related to this article can be found online at https://doi.org/10.1016/j.fct.2019.05.037.

References

Agger, K., Cloos, P.A., Christensen, J., Pasini, D., Rose, S., Rappsilber, J., Issaeva, I., Canaani, E., Salcini, A.E., Helin, K., 2007. UTX and JMJD3 are histone H3K27 demethylases involved in HOX gene regulation and development. Nature 449, 731–734.
Anglin, J.L., Song, Y., 2013. A medicinal chemistry perspective for targeting histone H3 lysine-79 methyltransferase DOT1L. J. Med. Chem. 56, 8972–8983.
Beauchamp, G.K., Keast, R.S., Morel, D., Lin, J., Pika, J., Han, Q., Lee, C.H., Smith, A.B., Breslin, P.A., 2005. Phytochemistry: ibuprofen-like activity in extra-virgin olive oil. Nature 437, 45–46.
Bindea, G., Mlecnik, B., Hackl, H., Charoentong, P., Tosolini, M., Kirilovsky, A., Fridman, W.H., Pagès, F., Trajanoski, Z., Galon, J., 2009. ClueGO: a Cytoscape plug-in to decipher functionally grouped gene ontology and pathwayannotation networks. Bioinformatics 25, 1091–1093.
Celano, M., Maggisano, V., Lepore, S.M., Russo, D., Bulotta, S., 2019. Secoiridoids of olive and derivatives as potential coadjuvant drugs in cancer: a critical analysis of experimental studies. Pharmacol. Res. 142, 77–86.
Colomer, R., Menéndez, J.A., 2006. Mediterranean diet, olive oil and cancer. Clin. Transl. Oncol. 8, 15–21.
Corominas-Faja, B., Cuyàs, E., Lozano-Sánchez, J., Cufí, S., Verdura, S., Fernández-Arroyo, S., Borrás-Linares, I., Martin-Castillo, B., Martin, Á.G., Lupu, R., Nonell-Canals, A., Sanchez-Martinez, M., Micol, V., Joven, J., Segura-Carretero, A., Menendez, J.A., 2018. Extra-virgin olive oil contains a metabolo-epigenetic inhibitor of cancer stem cells. Carcinogenesis 39, 601–613.
Corominas-Faja, B., Santangelo, E., Cuyàs, E., Micol, V., Joven, J., Ariza, X., Segura-Carretero, A., García, J., Menendez, J.A., 2014. Computer-aided discovery of biological activity spectra for anti-aging and anti-cancer olive oil oleuropeins. Aging (N Y) 6, 731–741.
Costanzo, P., Bonacci, S., Cariati, L., Nardi, M., Oliverio, M., Procopio, A., 2018. Simple and efficient sustainable semi-synthesis of oleacein [2-(3,4-hydroxyphenyl) ethyl (3S,4E)-4-formyl-3-(2-oxoethyl)hex-4-enoate] as potential additive for edible oils. Food Chem. 245, 410–414.
Cuyàs, E., Verdura, S., Llorach-Parés, L., Fernández-Arroyo, S., Joven, J., Martin-Castillo, B., Bosch-Barrera, J., Brunet, J., Nonell-Canals, A., Sanchez-Martinez, M., Menendez, J.A., 2018b. Metformin is a direct SIRT1-Activating compound: computational modeling and experimental validation. Front. Endocrinol. 9, 657.
Cuyàs, E., Verdura, S., Llorach-Pares, L., Fernández-Arroyo, S., Luciano-Mateo, F., Cabré, N., Stursa, J., Werner, L., Martin-Castillo, B., Viollet, B., Neuzil, J., Joven, J., Nonell-Canals, A., Sanchez-Martinez, M., Menendez, J.A., 2018 May 8a. Metformin directly targets the H3K27me3 demethylase KDM6A/UTX. Aging Cell e12772.
Escrich, E., Moral, R., Grau, L., Costa, I., Solanas, M., 2007. Molecular mechanisms of the effects of olive oil and other dietary lipids on cancer. Mol. Nutr. Food Res. 51, 1279–1292.
Feng, Q., Wang, H., Ng, H.H., Erdjument-Bromage, H., Tempst, P., Struhl, K., Zhang, Y., 2002. Methylation of H3-lysine 79 is mediated by a new family of HMTases without a SET domain. Curr. Biol. 12, 1052–1058.
Fernández del Río, L., Gutiérrez-Casado, E., Varela-López, A., Villalba, J.M., 2016. Olive oil and the hallmarks of aging. Molecules 21, 163.
Gimeno, A., Ojeda-Montes, M.J., Tomás-Hernández, S., Cereto-Massagué, A., Beltrán-Debón, R., Mulero, M., Pujadas, G., Garcia-Vallvé, S., 2019. The light and dark sides of virtual screening: what is there to know? Int. J. Mol. Sci. 20 pii: E1375.
Granchi, C., 2018. ATP citrate lyase (ACLY) inhibitors: an anti-cancer strategy at the crossroads of glucose and lipid metabolism. Eur. J. Med. Chem. 157, 1276–1291.
Hong, S., Moreno-Navarrete, J.M., Wei, X., Kikukawa, Y., Tzameli, I., Prasad, D., Lee, Y., Asara, J.M., Fernandez-Real, J.M., Maratos-Flier, E., Pissios, P., 2015. Nicotinamide N-methyltransferase regulates hepatic nutrient metabolism through Sirt1 protein stabilization. Nat. Med. 21, 887–894.
Hong, S., Zhai, B., Pissios, P., 2018. Nicotinamide N-methyltransferase interacts with enzymes of the methionine cycle and regulates methyl donor metabolism. Biochemistry 57, 5775–5779.
Hoshino, J., Kühne, U., Kröger, H., 1982. Methylation of nicotinamide in rat liver cytosol and its correlation with hepatocellular proliferation. Biochim. Biophys. Acta 719, 518–526.
Jin, C., Li, J., Green, C.D., Yu, X., Tang, X., Han, D., Xian, B., Wang, D., Huang, X., Cao, X., Yan, Z., Hou, L., Liu, J., Shukeir, N., Khaitovich, P., Chen, C.D., Zhang, H., Jenuwein, T., Han, J.D., 2011. Histone demethylase UTX-1 regulates C. elegans life span by targeting the insulin/IGF-1 signaling pathway. Cell Metabol. 14, 161–172.
Kim, W., Choi, M., Kim, J.E., 2014. The histone methyltransferase Dot1/DOT1L as a critical regulator of the cell cycle. Cell Cycle 13, 726–738.

Kim, W., Kim, R., Park, G., Park, J.W., Kim, J.E., 2012. Deficiency of H3K79 histone methyltransferase Dot1-like protein (DOT1L) inhibits cell proliferation. J. Biol. Chem. 287, 5588–5599.
Kraus, D., Yang, Q., Kong, D., Banks, A.S., Zhang, L., Rodgers, J.T., Pirinen, E., Pulinilkunnil, T.C., Gong, F., Wang, Y.C., Cen, Y., Sauve, A.A., Asara, J.M., Peroni, O.D., Monia, B.P., Bhanot, S., Alhonen, L., Puigserver, P., Kahn, B.B., 2014. Nicotinamide N-methyltransferase knockdown protects against diet-induced obesity. Nature 508, 258–262.
Lagunin, A., Filimonov, D., Poroikov, V., 2010. Multi-targeted natural products evaluation based on biological activity prediction with PASS. Curr. Pharmaceut. Des. 16, 1703–1717.
Lagunin, A., Stepanchikova, A., Filimonov, D., Poroikov, V., 2000. PASS: prediction of activity spectra for biologically active substances. Bioinformatics 16, 747–748.
Layne, J., Majkova, Z., Smart, E.J., Toborek, M., Hennig, B., 2011. Caveolae: a regulatory platform for nutritional modulation of inflammatory diseases. J. Nutr. Biochem. 22, 807–811.
Lombardo, G.E., Lepore, S.M., Morittu, V.M., Arcidiacono, B., Colica, C., Procopio, A., Maggisano, V., Bulotta, S., Costa, N., Mignogna, C., Britti, D., Brunetti, A., Russo, D., Celano, M., 2018. Effects of oleacein on high-fat diet-dependent steatosis, weight gain, and insulin resistance in mice. Front. Endocrinol. 9, 116.
López-Miranda, J., Pérez-Jiménez, F., Ros, E., De Caterina, R., Badimón, L., Covas, M.I., Escrich, E., Ordovás, J.M., Soriguer, F., Abiá, R., de la Lastra, C.A., Battino, M., Corella, D., Chamorro-Quirós, J., Delgado-Lista, J., Giugliano, D., Esposito, K., Estruch, R., Fernandez-Real, J.M., Gaforio, J.J., La Vecchia, C., Lairon, D., López-Segura, F., Mata, P., Menéndez, J.A., Muriana, F.J., Osada, J., Panagiotakos, D.B., Paniagua, J.A., Pérez-Martinez, P., Perona, J., Peinado, M.A., Pineda-Priego, M., Poulsen, H.E., Quiles, J.L., Ramírez-Tortosa, M.C., Ruano, J., Serra-Majem, L., Solá, R., Solanas, M., Solfrizzi, V., de la Torre-Fornell, R., Trichopoulou, A., Uceda, M., Villalba-Montoro, J.M., Villar-Ortiz, J.R., Visioli, F., Yiannakouris, N., 2010. Olive oil and health: summary of the II international conference on olive oil and health consensus report, Jaén and Córdoba (Spain) 2008. Nutr. Metabol. Cardiovasc. Dis. 20, 284–294.
Luo, W., Brouwer, C., 2013. Pathview: an R/Bioconductor package for pathway-based data integration and visualization. Bioinformatics 29, 1830–1831.
Maures, T.J., Greer, E.L., Hauswirth, A.G., Brunet, A., 2011. The H3K27 demethylase UTX-1 regulates C. elegans lifespan in a germline-independent, insulin-dependent manner. Aging Cell 10, 980–990.
Menendez, J.A., Joven, J., Aragonès, G., Barrajón-Catalán, E., Beltrán-Debón, R., Borrás-Linares, I., Camps, J., Corominas-Faja, B., Cufí, S., Fernández-Arroyo, S., Garcia-Heredia, A., Hernández-Aguilera, A., Herranz-López, M., Jiménez-Sánchez, C., López-Bonet, E., Lozano-Sánchez, J., Luciano-Mateo, F., Martin-Castillo, B., Martin-Paredero, V., Pérez-Sánchez, A., Oliveras-Ferraros, C., Riera-Borrull, M., Rodríguez-Gallego, E., Quirantes-Piné, R., Rull, A., Tomás-Menor, L., Vazquez-Martin, A., Alonso-Villaverde, C., Micol, V., Segura-Carretero, A., 2013. Xenohormetic and anti-aging activity of secoiridoid polyphenols present in extra virgin olive oil: a new family of gerosuppressant agents. Cell Cycle 12, 555–578.
Menendez, J.A., Lupu, R., 2006. Mediterranean dietary traditions for the molecular treatment of human cancer: anti-oncogenic actions of the main olive oil's monounsaturated fatty acid oleic acid (18:1n-9). Curr. Pharmaceut. Biotechnol. 7, 495–502.
Menendez, J.A., Vazquez-Martin, A., Garcia-Villalba, R., Carrasco-Pancorbo, A., Oliveras-Ferraros, C., Fernandez-Gutierrez, A., Segura-Carretero, A., 2008. tabAnti-HER2 (erbB-2) oncogene effects of phenolic compounds directly isolated from commercial Extra-Virgin Olive Oil (EVOO). BMC Canc. 8, 377.
Menendez, J.A., Vazquez-Martin, A., Oliveras-Ferraros, C., Garcia-Villalba, R., Carrasco-Pancorbo, A., Fernandez-Gutierrez, A., Segura-Carretero, A., 2009. Extra-virgin olive oil polyphenols inhibit HER2 (erbB-2)-induced malignant transformation in human breast epithelial cells: relationship between the chemical structures of extra-virgin olive oil secoiridoids and lignans and their inhibitory activities on the tyrosine kinase activity of HER2. Int. J. Oncol. 34, 43–51.
Nardi, M., Bonacci, S., De Luca, G., Maiuolo, J., Oliverio, M., Sindona, G., Procopio, A., 2014. Biomimetic synthesis and antioxidant evaluation of 3,4-DHPEA-EDA [2-(3,4-hydroxyphenyl) ethyl (3S,4E)-4-formyl-3-(2-oxoethyl)hex-4-enoate]. Food Chem. 162, 89–93.
Nguyen, A.T., Zhang, Y., 2011. The diverse functions of Dot1 and H3K79 methylation. Genes Dev. 25, 1345–1358.
Ortegren, U., Aboulaich, N., Ost, A., Strålfors, P., 2007. A new role for caveolae as metabolic platforms. Trends Endocrinol. Metabol. 18, 344–349.
Pang, K.L., Chin, K.Y., 2018. The biological activities of oleocanthal from a molecular perspective. Nutrients 10 (5) pii: E570.
Peleg, S., Feller, C., Forne, I., Schiller, E., Sévin, D.C., Schauer, T., Regnard, C., Straub, T., Prestel, M., Klima, C., Schmitt Nogueira, M., Becker, L., Klopstock, T., Sauer, U., Becker, P.B., Imhof, A., Ladurner, A.G., 2016. Life span extension by targeting a link between metabolism and histone acetylation in Drosophila. EMBO Rep. 17, 455–469.
Pérez-Jiménez, F., Ruano, J., Perez-Martinez, P., Lopez-Segura, F., Lopez-Miranda, J., 2007. The influence of olive oil on human health: not a question of fat alone. Mol. Nutr. Food Res. 51, 1199–1208.
Piroddi, M., Albini, A., Fabiani, R., Giovannelli, L., Luceri, C., Natella, F., Rosignoli, P., Rossi, T., Taticchi, A., Servili, M., Galli, F., 2017. Nutrigenomics of extra-virgin olive oil: a review. Biofactors 43, 17–41.
Reboredo-Rodríguez, P., Varela-López, A., Forbes-Hernández, T.Y., Gasparrini, M., Afrin, S., Cianciosi, D., Zhang, J., Manna, P.P., Bompadre, S., Quiles, J.L., Battino, M., Giampieri, F., 2018. Phenolic compounds isolated from olive oil as nutraceutical tools for the prevention and management of cancer and cardiovascular diseases. Int. J. Mol. Sci. 19 pii: E2305.
Santos, A.L., Lindner, A.B., 2017. Protein posttranslational modifications: roles in aging and Age-related disease. Oxid Med Cell Longev 2017, 5716409.
Shah, P.P., Donahue, G., Otte, G.L., Capell, B.C., Nelson, D.M., Cao, K., Aggarwala, V., Cruickshanks, H.A., Rai, T.S., McBryan, T., Gregory, B.D., Adams, P.D., Berger, S.L., 2013. Lamin B1 depletion in senescent cells triggers large-scale changes in gene expression and the chromatin landscape. Genes Dev. 27, 1787–1799.
Shannon, P., Markiel, A., Ozier, O., Baliga, N.S., Wang, J.T., Ramage, D., Amin, N., Schwikowski, B., Ideker, T., 2003. Cytoscape: a software environment for integrated models of biomolecular interaction networks. Genome Res. 13, 2498–2504.
SRERE, P.A., 1959. The citrate cleavage enzyme. I. Distribution and purification. J. Biol. Chem. 234, 2544–2547.
Stepanchikova, A.V., Lagunin, A.A., Filimonov, D.A., Poroikov, V.V., 2003. Prediction of biological activity spectra for substances: evaluation on the diverse sets of drug-like structures. Curr. Med. Chem. 10, 225–233.
Ulanovskaya, O.A., Zuhl, A.M., Cravatt, B.F., 2013. NNMT promotes epigenetic remodeling in cancer by creating a metabolic methylation sink. Nat. Chem. Biol. 9, 300–306.
Vanhooren, V., Navarrete Santos, A., Voutetakis, K., Petropoulos, I., Libert, C., Simm, A., Gonos, E.S., Friguet, B., 2015. Protein modification and maintenance systems as biomarkers of ageing. Mech. Ageing Dev. 151, 71–84.
Vazquez-Martin, A., Fernández-Arroyo, S., Cufí, S., Oliveras-Ferraros, C., Lozano-Sánchez, J., Vellón, L., Micol, V., Joven, J., Segura-Carretero, A., Menendez, J.A., 2012. Phenolic secoiridoids in extra virgin olive oil impede fibrogenic and oncogenic epithelial-to-mesenchymal transition: extra virgin olive oil as a source of novel antiaging phytochemicals. Rejuvenation Res. 15, 3–21.
Verdura, S., Cuyàs, E., Llorach-Parés, L., Pérez-Sánchez, A., Micol, V., Nonell-Canals, A., Joven, J., Valiente, M., Sánchez-Martínez, M., Bosch-Barrera, J., Menendez, J.A., 2018a. Silibinin is a direct inhibitor of STAT3. Food Chem. Toxicol. 116, 161–172.
Verdura, S., Cuyàs, E., Lozano-Sánchez, J., Bastidas-Velez, C., Llorach-Parés, L., Fernández-Arroyo, S., Hernández-Aguilera, A., Joven, J., Nonell-Canals, A., Bosch-Barrera, J., Martin-Castillo, B., Vellon, L., Sanchez-Martinez, M., Segura-Carretero, A., Menendez, J.A., 2019. An olive oil phenolic is a new chemotype of mutant isocitrate dehydrogenase 1 (IDH1) inhibitors. Carcinogenesis 40, 27–40.
Visioli, F., Bernardini, E., 2011. Extra virgin olive oil's polyphenols: biological activities. Curr. Pharmaceut. Des. 17, 786–804.
Wellen, K.E., Hatzivassiliou, G., Sachdeva, U.M., Bui, T.V., Cross, J.R., Thompson, C.B., 2009. ATP-citrate lyase links cellular metabolism to histone acetylation. Science 324, 1076–1080.
Xu, X., Huang, M., Zou, X., 2018. Docking-based inverse virtual screening: methods, applications, and challenges. Biophys Rep 4, 1–16.
Zaidi, N., Swinnen, J.V., Smans, K., 2012. ATP-citrate lyase: a key player in cancer metabolism. Cancer Res. 72, 3709–3714.
Zhao, S., Torres, A., Henry, R.A., Trefely, S., Wallace, M., Lee, J.V., Carrer, A., Sengupta, A., Campbell, S.L., Kuo, Y.M., Frey, A.J., Meurs, N., Viola, J.M., Blair, I.A., Weljie, A.M., Metallo, C.M., Snyder, N.W., Andrews, A.J., Wellen, K.E., 2016. ATP-citrate lyase controls a glucose-to-Acetate metabolic switch. Cell Rep. 17, 1037–1052.